DOI: 10.1021/ma901093u

Macromolecules
ARTICLE

# Microphase Separation of Mixed Binary Polymer Brushes at Different Temperatures

**Gui-Li He,*,†,‡ Holger Merlitz,†,§ Jens-Uwe Sommer,§ and Chen-Xu Wu†**

†*Department of Physics and Institute of Theoretical Physics and Astrophysics, Xiamen University, Xiamen 361005, P.R. China,* ‡*Institut für Theoretische Physik II, Heinrich-Heine-Universität Düsseldorf, Universitätsstrasse 1, D-40225 Düsseldorf, Germany, and* §*Leibniz-Institut für Polymerforschung Dresden, 01069 Dresden, Germany*

*Received May 19, 2009; Revised Manuscript Received August 3, 2009*

ABSTRACT: The microphase separation of binary polymer brushes at different temperatures is studied via Langevin molecular dynamics simulations. The order−disorder transition (ODT) from a homogeneous state to microphase-separated structures is investigated by analyzing various system properties such as the composition (density) distribution, lateral displacement of chain conformation, vertical center of mass, structure factor, and pair-correlation function. In an attempt to regularize the stripe pattern of microphase domains, the impact of solvent flow on the domain pattern is investigated.

## I. Introduction

Polymer brushes consist of linear macromolecules that are attached with one end onto a substrate. Their potential applications are widely spread over various fields, including superhydrophobic coatings,[1] antifriction coatings,[2] or adhesion,[3] to cite just a few of them. Recent experiments[4−6] have investigated the switchable properties of binary brushes which compose of hydrophilic and hydrophobic homopolymer components. The microphase segregation of mixed binary polymer brushes is also observed in the laboratory.[7,8]

Using both a Flory-type mean-field approach and scaling arguments, the phase diagram of a grafted (laterally mobile) binary monolayer has been investigated by Halperin.[9] The system was found to behave like a two-dimensional regular solution with an interaction parameter depending on the grafting density. Later on, a theoretical analysis of microphase separation in binary micelles, composed of two chemically distinct polymeric surfactants, was studied.[10] In that work, both intramicellar and intermicellar processes were analyzed in detail. Furthermore, mixed binary polymer brushes have also been approached theoretically by Marko and Witten, who investigated the phase diagrams of these systems via self-consistent-field theory (SCF) in the strong stretching limit.[11,12] Their approach was later generalized to brushes of arbitrary grafting density by Müller, who has observed diverse morphological configurations of microphase separations.[13] In addition, it is also known that the designing patterned surfaces by grafting Y-shaped copolymers were discussed by using scaling arguments.[14] Their work was mainly on how solvent quality, grafting density, and chain length affect the structure of the grafted layer.

A first theoretical analysis of the ODT from a homogeneous melt to microphase-separated phase was done by Leibler[15] with the method of random phase approximation; he employed a Landau-type mean-field theory (MFT) to locate the ODT and evaluated the structure factor and the phase diagram. This MFT was extended to include the impact of fluctuations by Fredrickson and Helfand. A modified phase diagram and additional chain-length-dependent modifications of the MFT have been achieved through first-order Hartree corrections.

Because of the neglect of thermal fluctuations, the SCF approach often predicts highly regular patterns for the microphase separation of mixed brushes. Taking the fluctuations into account via computer simulations, Soga et al. were among the first to simulate and investigate properties of the microphase separation of binary brushes at different solvent qualities.[16] Subsequently, Monte Carlo simulations were employed by Wenning et al. to investigate the brush structure as a function of the grafting pattern.[17] Including different solvent qualities, the influence of the particular grafting morphology on the microphase domain structure was simulated and analyzed by Santer et al.,[18] and the switching of mixed brushes with hydrophilic/hydrophobic upon change of solvent quality has recently been analyzed by the authors.[19]

The primary scope of the present work was to study the ODT of the binary brush using a couple of different analysis tools and to investigate how the microphase domain patterns could be engineered with the help of a shear flow. A polymer brush with a regular stripe pattern would serve as an interesting substrate to investigate the adsorption behavior of polymers on a surface with nanoscale regular potential. There exist recent theoretical studies of such systems which are worth being investigated experimentally.[20] In section II the polymer model parameters and the procedure of simulations are explained. Section III discusses the structural properties and ODT temperature of the brush system at grafting density $\sigma = 0.12$ and chain length $N = 64$. In section IV the impact of shear is analyzed for $\sigma = 0.12$ and $T = 0.5$. A summary of our work is presented and discussed in the last section (section V).

## II. Methodology

**A. Model.** The polymer chains were modeled as series of coarse-grained bead−spring monomers without bending potential or explicit twist; i.e., the bonds were freely rotating and freely jointed within the limits as confined by excluded volume interactions with the neighboring monomers. The finite extensible nonlinear elastic (FENE) potential[21] was

*Corresponding author. E-mail: guili@thphy.uni-duesseldorf.de.

 Published on Web 08/27/2009 © 2009 American Chemical Society

used to create the connectivity between the represented spherical Kuhn monomers by the beads. The pair interaction between monomers was a shifted Lennard-Jones (LJ) potential:

$$U_{\mathrm{LJ}}(r) = 4\epsilon\left[\left(\frac{\sigma_\mathrm{b}}{r}\right)^{12} - \left(\frac{\sigma_\mathrm{b}}{r}\right)^{6} - \left(\frac{\sigma_\mathrm{b}}{r_\mathrm{c}}\right)^{12} + \left(\frac{\sigma_\mathrm{b}}{r_\mathrm{c}}\right)^{6}\right] \quad (1)$$

Here $\epsilon$ is the bead−bead interaction strength, $\sigma_\mathrm{b}$ stands for the bead size, and the parameter $r_\mathrm{c}$ is the cutoff distance. It is easily deduced that, when $r_\mathrm{c}$ goes to infinity, the potential will have a minimum at $r_\mathrm{min} = 2^{1/6}\sigma_\mathrm{b}$ with the depth $U_{\mathrm{LJ}}(r_\mathrm{min}) = -\varepsilon$. Herein, once a cutoff $r_\mathrm{c} = 2^{1/6}\sigma_\mathrm{b}$ is implemented, only the repulsive contribution remains, and in this way we could simulate the monomers in an athermal solvent. Furthermore, a far cutoff retains the attractive part of the LJ potential and allows to model diverse solvent qualities which are dependent on both the interaction strength ($\epsilon$) and the temperature ($T$) of the system. In this way, $\epsilon$ and $T$ can take over some parts of the solvent selectivity within this implicit solvent model. Unless athermal solvent has to be simulated, it is common practice to select $r_\mathrm{c} = 2.5\sigma_\mathrm{b}$ in order to keep the number of pair interactions on a tolerable level. The influence of the temperature on the quality of the solvent will be described in the results section.

In the model, the binary brush contained two kinds of homopolymer chains and end-grafted to form a 24 × 24 grid on a flat surface which defined an $x-y$ plane. The $z$ direction is vertical to this planar surface and points to the space in which the chains existed. Periodic boundary conditions were applied in the $x-y$ direction, whereas the grafting surface was located at $z = 0$ which was featuring a short-range repulsive 9−3 type LJ wall potential

$$U_\mathrm{wall} = \epsilon\left[\frac{2}{15}\left(\frac{\sigma_\mathrm{b}}{r}\right)^{9} - \left(\frac{\sigma_\mathrm{b}}{r}\right)^{3}\right] \quad (2)$$

Here with cutoff at its minimum and a subsequent shift up, the potential had only repulsive contributions remaining to prevent the monomers from passing through the grafting substrate. The two polymer species consisted of monomers which henceforth shall be denoted as A type and B type, respectively. In this work we have used Cartesian grafting patterns (grids), both a checkerboard (i.e., each grafted A monomer has got four next neighbors of B type) and an alternation of rows of A and B (i.e., each grafted A monomer has got two next neighbors of either type). The two grafted species of the binary brushes in this work took this alternative way to fit on the checkerboard except for the brushes in section IV, where the randomly grafting way was simulated as well to compare with the results which were obtained in the alternative method. In that part, the grafting monomers were still taken the Cartesian pattern, but the two species had the same probability to be chosen as spatial neighbors. In all the models, both polymer species were of identical volume fractions and identical number of repeat units (chain length) $N = 64$. In this work, the A−B interaction did not contain any attractive contribution and the wall potential did not distinguish between both species. For interaction among the same species i.e., A−A or B−B, attractive interactions are considered.

To simulate the binary brushes, the open source LAMMPS molecular dynamics package[22] was employed. The LJ potential in eq 1 defines the LJ set of units, featuring a bead diameter $\sigma_\mathrm{b} = 1$ (one length unit), a potential depth $\epsilon = 0.25$ (one energy unit), and a mass $m = 1$ (one mass unit). Note that with the choice $\epsilon = 0.25$ it might be adequate to define an effective temperature $T^* = T/\epsilon = 4T$, where $T$ is the system temperature in units of the Boltzmann constant. In order to remain consistent with previous publications,[19] however, we do consequently refer to $T$ instead of the effective $T^*$ throughout this paper. With this choice of units, the $\Theta$ temperature of the system is located around $T_\Theta \approx 0.75$.[19]

The grafting density $\sigma$ of the binary polymer brush is defined as the (average) number of grafted monomers per unit area. If the monomer size were set as $\sigma_\mathrm{b} = 1$, the grafting density of $\sigma = 1$ would create a closely packed polymer crystal.[23] The FENE attractive bond potential allowed a maximum bond length of $R_0 = 1.5\sigma_\mathrm{b}$, and the spring constant was chosen to be $K = 60\varepsilon/\sigma_\mathrm{b}^2$ in order to withstand the strong fluctuations of monomers at high temperatures. (For uncharged chains, the parameter set leds to an average bond length of $l_\mathrm{av} \approx 0.97\sigma_\mathrm{b}$.)

The equation of motion of every nongrafted monomer in the implicit solvent (neglecting any hydrodynamic interaction) is given by the Langevin equation:

$$m\frac{\mathrm{d}^2\mathbf{r}_i}{\mathrm{d}t^2} + \zeta\frac{\mathrm{d}\mathbf{r}_i}{\mathrm{d}t} = -\frac{\partial U}{\partial \mathbf{r}_i} + \mathbf{F}_i \quad (3)$$

where $m = 1$ is the monomer mass, $\mathbf{r}_i$ is the position of the $i$th monomer, $U$ is the total conservative potential, and $\mathbf{F}_i$ is a random external force without drift and a second moment proportional to the temperature and the friction constant $\zeta$. The parameter settings for the dynamics were identical with previous simulations.[19]

**B. Simulation Procedure.** The initial brush configuration was set up as an array of stretched chains. Then several $10^6$ MD steps were carried out for relaxation of the brush at highest temperature which was chosen to be of $T = 5.0$ in our work, followed by a slow gradual decrease of the temperature down to the lowest value $T = 0.5$. In between, the states of the brush were stored regularly in order to serve as initial states for new trajectories, computed at different but constant temperatures.

We used the following parameters for our analysis: At grafting density $\sigma = 0.12$: $T \in \{5.0, 3.2, 2.75, 2.3, 1.4, 0.85, 0.5\}$, at $\sigma = 0.32$: $T \in \{5.0, 4.0, 3.0, 2.0, 1.5, 1.0, 0.5\}$, and at $\sigma = 0.6$: $T \in \{5.0, 3.34, 2.51, 1.68, 0.85, 0.5\}$. Qualitative differences between the domain patterns at different temperatures are displayed in Figure 1. It is obvious that a transition from disorder to order takes place while decreasing the temperature. Furthermore, it is obvious as well as that the transition temperature depends on grafting density: At high grafting densities (lower panels), a certain amount of order remains visible even at the highest temperatures. In any case the morphologies at lower temperatures appear to be better ordered. In the following sections, we analyze this transition from disorder (homogeneous mixing) to order (separation into microphase domains) in a systematic manner using various approaches.

## III. Results

**A. Visualization of the Composition and Density Distributions.** Figure 2 displays the time-averaged density distributions and the corresponding composition distributions of the brush ($\sigma = 0.12$) at four selected temperatures ($T \in \{3.2, 2.3, 0.85, 0.5\}$). All plots in Figure 2 are monomer densities averaged over thousands of configurations after the system was given enough time to equilibrate. The vertical ($z-$) direction is pointing from the bottom (substrate) to the top (brush surface), and the horizontal cross sections in each subfigures are parallel to the substrate ($x-y$ plane).

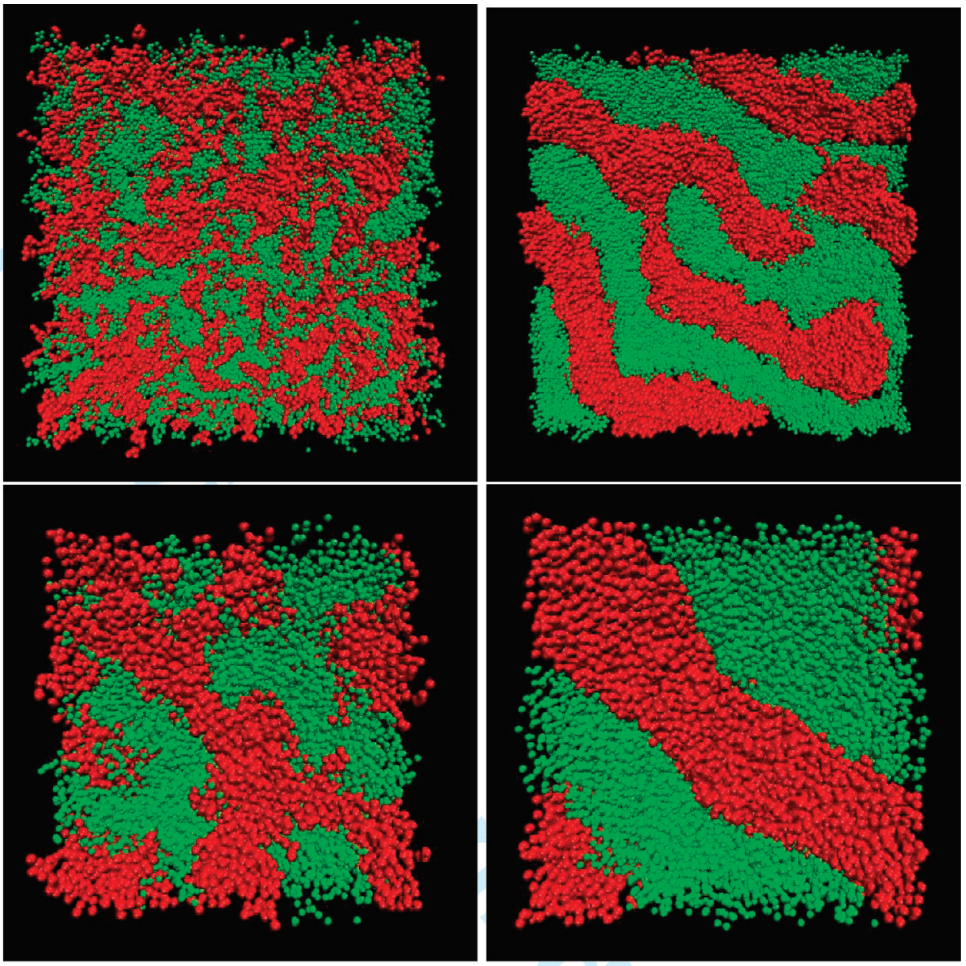

**Figure 1.** Snapshots (top view) of microphase-separated polymer brushes. Here the upper two pictures show binary brushes at grafting density $\sigma = 0.12$, at temperature $T = 5.9$ (left), and $T = 0.5$ (right). The lower panels are for $\sigma = 0.6$, $T = 5.0$ (left) and $T = 0.5$ (right).

At high temperatures, the densities display a certain degree of local fluctuations, but extended microphase domains remain absent. Microphase domains are emerging around $T = 2.3$ which are forming an irregular pattern of stripes extending over spacial dimensions similar to the system size. Near the phase boundaries, the monomer density is significantly reduced. The latter phenomenon becomes even more pronounced at temperatures below the theta point, which is located near $T = 0.75$. The theta temperature is identical for both monomer species because the (implicit) solvent was nonselective. At $T = 0.5$, the brush layer has collapsed, and the different incompatible microdomains are forming three-dimensional droplike structures as a result of their surface tension.

The figures indicate that the ODT extends over a range of temperatures, an observation similar to previous findings for the microphase separation of diblock copolymers.[24] This fact might be the result of finite system size combined with a first-order-like nature of the ODT as known also for symmetric diblock copolymers. We note, however, that in contrast to microphase separation in block copolymers, the chains of a brush are fixed and hence no translational entropy is involved in the transition. For the same reason, the system has got no chance to form macroscopically separated phases, and the interaction energy at the phase boundaries is never becoming negligible and does change only gradually with the domain size. While the temperature is decreased, chains of the same species are also bending aside to form microdomains (Figure 5, inset), and this process generates a free energy penalty due to reduction of conformational entropy. Being of entropic nature, this penalty itself is temperature-dependent, and this might be one reason for the fact that the microdomains keep on growing upon further temperature reduction.

**B. Structure Factor and Weak Segregation Analysis.** The experimental determination of the geometry and morphology of polymer brushes is usually based on scattering and reflectivity measurements and especially on the static structure factor $S(\mathbf{q})$, where $\mathbf{q}$ denotes the scattering vector.[24,25] We calculate the structure factor as follows:

$$S(\mathbf{q}) = \frac{1}{N_m}\langle \sum_{s,l=1}^{N_m} \sigma_s \sigma_l \exp[i\mathbf{q}(\mathbf{r}_s - \mathbf{r}_l)]\rangle \qquad (4)$$

Here the sum runs over all $N_m$ monomers with coordinates $\mathbf{r}_s$, which were restricted to the horizontal upper half layer of the brush. The average is obtained from 2000 conformations along the system trajectory. The contrast factors $\sigma_s$ (or $\sigma_l$) are taking spin-type values $\pm 1$, depending on the monomer species. Since the phase separation occurs in lateral direction, we compute the structure factor for the $xy$-plane. The periodic boundary condition of the simulation box in both lateral directions is limiting the choices for the scattering vector to

$$\mathbf{q}_{xy} = \frac{2\pi}{L}(n_x, n_y), \quad 0 \le n_i \le L \qquad (5)$$

with $L$ being the box size. To increase the statistics of our results, we calculate the isotropic average: The structure factor

is calculated for all possible **q** vectors and then averaged over those of equal length.

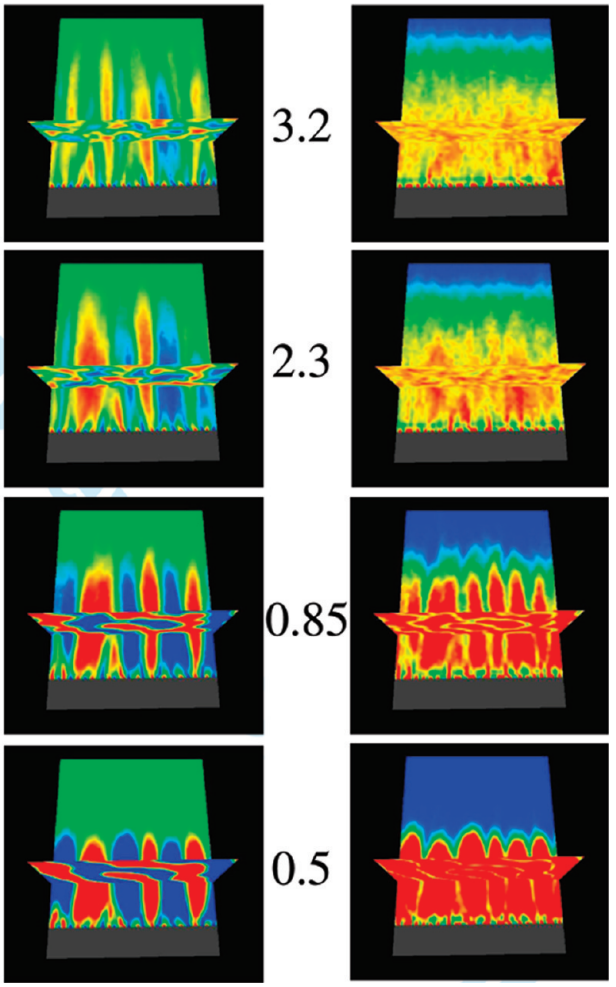


**Figure 2.** 3-dimensional density distributions (right column) and composition density distributions (left column) of the binary polymer brush ($\sigma$ = 0.12) at four selected temperatures, ranging from $T$ = 0.5 to $T$ = 3.2.

Our results are presented in Figure 3. Generally, when the temperatures are above 2.75, the structure factors are almost flat, which implies that the monomers are forming a disordered and nearly homogeneous phase. Peaks are emerging around $T$ = 2.75 and becoming increasingly pronounced with decreasing temperatures, indicating the creation of the microphase domain structure.

In order to estimate the ODT, we employ a formal analogy with microphase separation in symmetric block copolymers. Using the Leibler theory close to the ODT, Hoffmann et al.[24] have used the following relation:

$$\frac{1}{S(\mathbf{q})_{max}} \sim \frac{1}{T_{sp}} - \frac{1}{T} \tag{6}$$

where $T_{sp}$ is the spinodal temperature at which $S(\mathbf{q})_{max}$ diverges.[25] In the mean-field theory, this spinodal temperature coincides with the ODT, i.e., $T_{sp} = T_{ODT}$. The fluctuations above the ODT prevent the divergence of $S(\mathbf{q})_{max}$ and a nonlinear relation between $S(\mathbf{q})_{max}^{-1}$ and $T^{-1}$ is induced, which is discussed in eq 8 of ref 24 and in the original reference.[26] The inset of Figure 3 displays the inverse maximum of the structure factor ($S(\mathbf{q})_{max}^{-1}$) as a function of the inverse temperature ($T^{-1}$). At high temperature, $S(\mathbf{q})_{max}^{-1}$ depends linearly on $T^{-1}$, and it can be extrapolated to the intersection with the abscissa to estimate the location of the ODT. Using eq 6 in the form $S(\mathbf{q})_{max}^{-1} = a_0 + a_1 \times T^{-1}$ which is fitted to the high temperature data, we obtain the parameters $a_0$ = 0.04 and $a_1$ = −0.09. Therefore, we have $T_{ODT}^{-1} = -a_0/a_1$, so that $T_{ODT} \approx 2.3$. The fact that this construction delivers a well-defined value for $T_{ODT}$ does not imply that the transition actually does take place at exactly that point or any other well-defined temperature. Instead, the transition is smooth, and $T_{ODT} \approx 2.3$ is merely the result of a formal procedure, though consistent with the previously made qualitative observations.

**C. Pair-Correlation Function.** Complementary to the structure factor, the pair-correlation function may be analyzed. While the structure factor is analyzing properties of the system in $k$-space and, in particular, displays long-range periodic structures as strong peaks, the pair correlations are more explicit about the short-range properties of the system

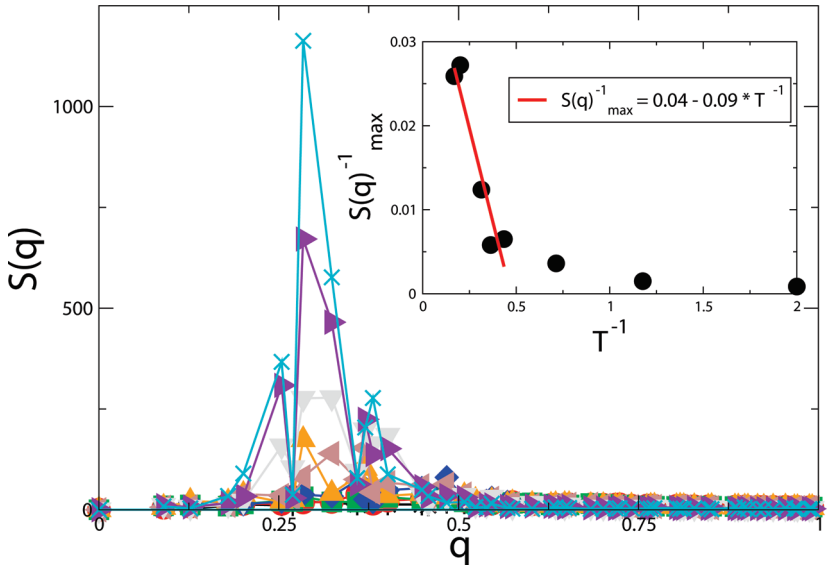


**Figure 3.** The lateral, radially averaged structure factor $S(\mathbf{q})$ for a binary brush ($N$ = 64 and $\sigma$ = 0.12) at different temperatures. The cross symbols stand for $T$ = 0.5, right triangles for $T$ = 0.85, down triangles for $T$ = 1.4, left triangles for $T$ = 2.3, and up triangles for $T$ = 2.75. At higher temperatures, the peaks are diminishing. Inset: plot of the inverse maximum peak intensity $S(\mathbf{q})_{max}^{-1}$ as a function of inverse temperature $T^{-1}$. Here, the solid line shows the fit function $S(\mathbf{q})_{max}^{-1} = 0.04 - 0.09 \times T^{-1}$.

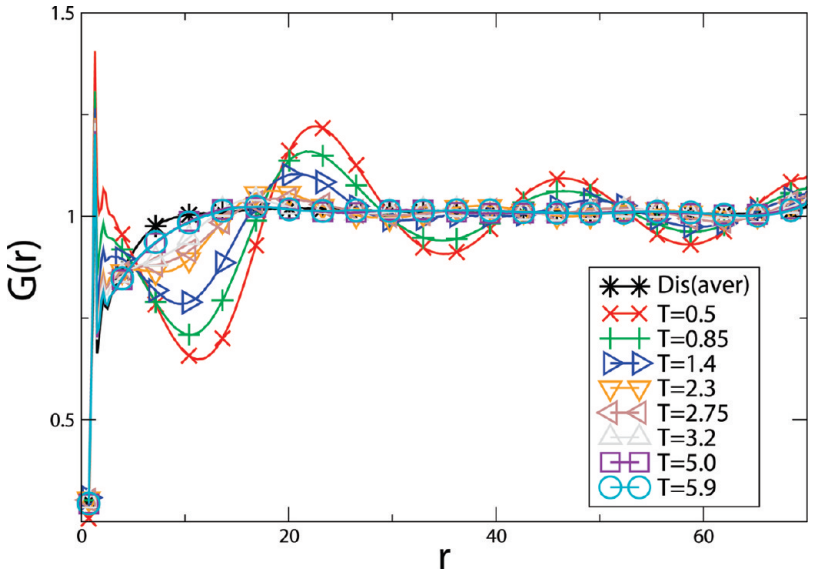


**Figure 4.** Plot of the pair-correlation function, defined in eq 7, at different temperatures averaged over type A and B species. For the computation, only the monomers inside the upper half part of the brush are taken into account. For comparison, the stars correspond to a fully disordered system containing two species with identical pair interaction.

in real space. We define the lateral pair correlation function as follows:

$$G(r) = \frac{\rho_r}{\rho_0} \tag{7}$$

where $\rho_r$ is the average density at lateral distance $r$ from a given monomer and $\rho_0$ is the average density within the volume of lateral radius $r$, both computed in the upper half layer in the lateral directions for each species, and then we obtain the $G(r)$ for each type of the chain. Finally, the average $G(r)$ over both species is taken.

Figure 4 contains the pair-correlation functions obtained in this way at different temperatures. Generally, there is a large amplitude at small distance ($r$) for all temperatures, the result of a short-range ordering generated by the monomer at the origin. At low temperatures, further oscillations appear which extend over larger distances, indicating a long-range ordering created by the microphase domain structure. These oscillations remain absent at high temperatures and, for comparison, in the case of a fully disordered system in which both species are indistinguishable (stars). These oscillations are still discernible at $T = 1.4$ (right triangles), but not anymore at $T = 2.3$, indicating that the long-range order emerges somewhere within this temperature range. At short distances, the oscillation amplitudes remain to depend on $T$ even at rather high temperatures, which indicates that on short length scales a local ordering takes present at higher temperatures. This is also consistent with Figure 1, in which small clusters of like species appear to exist even at the highest simulation temperature. It is clearly observable how the ODT is taking place on different length scales: first, i.e. at rather high temperature, a local ordering is taking place, and then, upon further lowering the temperature, a long-range order is created.

**D. Height and Lateral Deviation.** The average lateral deviation

$$\langle |R_{xy}| \rangle = \langle \sqrt{(x_N - x_1)^2 + (y_N - y_1)^2} \rangle \tag{8}$$

of the end monomer $(x_N, y_N)$ from the grafting point $(x_1, y_1)$ and the thickness of the brush layer are investigated in this section. $|R_{xy}|$ is evaluated for each chain and then averaged over all $24 \times 24$ chains and thousands of configurations. The results for brushes at various temperatures and at different grafting densities ($\sigma \in \{0.12, 0.32, 0.6\}$) are displayed in Figure 5. This figure shows that the average lateral deviations for $\sigma = 0.12$ (circles) remain almost constant at temperatures beyond $T = 2.3$, but they increase once the temperature is dropping below that value. The increase of lateral deviations is a consequence of the microphase separation, during which single chains are forced to bend aside into phase domains of like species. Consistent with the analysis of the previous section, the transition temperature appears to be close to $T \approx 2.3$.

At this stage it is instructive to take a look at brushes which are grafted at high densities. Figure 5 also contains data for $\sigma = 0.32$ (squares) and $\sigma = 0.6$ (diamonds). Here, the lateral deviations continue to drop up to rather high temperatures around $T = 5$. As was visible already in Figure 1, microphase domains continue to exist even at high temperatures and do just gradually change their sizes. Here, the ODT appears to be a very smooth and gradual transition as a function of temperature. One has to consider the fact that at high grafting densities the interaction energy per chain is much higher than it is at low density, and each chain has got plenty of interactions with unlike chains which are grafted nearby, at least in the lower region of the brush, near the substrate. Hence, the surface energy of the phase domains delivers an important contribution to the total energy of the system. Moreover, the entropy of the brush is very low at high grafting densities, and it would require rather high temperatures for the entropic contribution to dominate the free energy and create a homogeneous mixture. A complete mixing has therefore not been observed at these densities and within the range of temperatures considered in this simulations.

The inset additionally displays the layer thickness $H$ of the brush as a function of temperature. Here, $\langle H \rangle$ was evaluated as the vertical center-of-mass coordinate of the polymer layer. This quantity coincides with both polymer species because the solvent is nonselective. At low grafting densities (circles) the ODT appears to have just a marginal influence on brush height: Between $T = 1.5$ and $T = 2.3$ the height is

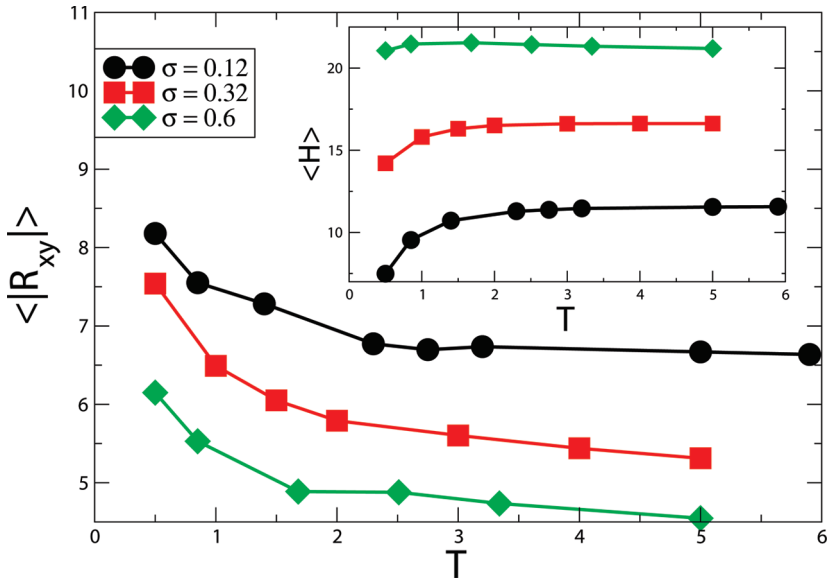


**Figure 5.** Plot of the average lateral deviation of the end monomer $(x_N, y_N)$ from the grafting point $(x_1, y_1)$ against the temperature. Inset: the average layer thickness (vertical center of mass) plotted against the temperature.

increasing by a little amount. A sharp increase, however, occurs at $0.5 < T < 1$ when the system is passing through its theta point.

At high grafting densities, the brush is hardly collapsing during the theta transition because of the strong (higher order) excluded volume effects. It is interesting to note that at very high density, $\sigma = 0.6$, the brush height is decreasing once the system is in good solvent and the temperature is further increased. As a result of thermal fluctuations, the strongly stretched chains retreat a little bit to increase their conformational entropy, thereby creating a negative thermal expansion coefficient.[27]

**E. The Vassiliev−Matsen Order Parameter.** The ODT is a gradual process so that it is no trivial task to identify significant differences between the disordered state and the ordered state close to the transition. The structure function as considered in section IIIB may serve as an order parameter. In particular, the occurrence of higher order Bragg reflexes can be taken as a signature of the (long-range) ordered state.[24] However, disorder in the lamellar morphology can obscure this effect and can lead to an underestimation of the transition temperature. In reference,[28] Vassiliev and Matsen suggested an alternative order parameter $\psi$ motivated by their investigation of the ODT in block copolymers. The system is partitioned into a lattice of $N_{tot}$ sites, the size of which being of the order of the monomer size, and the occupancy of each lattice site is analyzed. Then, the quantity

$$\psi = \frac{1}{{N_{tot}}^2} \sum_{i \neq j}^{N_{tot}} {V_{ij}}^2 \tag{9}$$

in which $V_{ij}$ is the correlation function

$$V_{ij} = \langle \sigma_i \sigma_j \rangle - \langle \sigma_i \rangle^2 \tag{10}$$

and $i, j \in \{1, 2, ..., N_{tot}\}$, $N_{tot}$ being the total number of lattice sites. The quantity $\langle \sigma_i \rangle = \phi_c(N_A - N_B)/N_{tot}$, in which $\phi_c$ is the total monomer occupancy and $N_A$ ($N_B$) the number of A species (B species), equals zero in our system because of the symmetry $N_A = N_B$. Theoretically, the order parameter should assume a small positive value in the disordered phase, which approaches zero for infinite system size, and a reasonably large value, independent of system size, in the ordered phase. The values of this order parameter computed for the entire brushes at different temperatures are plotted in Figure 6. As expected, this order parameter is larger at low temperatures, then, with increasing temperature, dropping sharply to a low value where it stays almost constant. According to this order parameter, the ODT appears to take place at lower temperatures when compared with the results in previous sections. While the analysis of the structure factor and the lateral deviations suggested a value $T_{ODT} \approx 2.3$, the order parameter of this section appears to suggest $T_{ODT} < 1.5$ instead.

The explanation for this unexpected result is found when considering that the quantity $\langle \sigma_i \sigma_j \rangle$ depends on the fluctuation behavior of the monomers. If the monomers were moving freely through the system, then a proper ensemble average of this quantity would approach zero. On the other hand, frozen monomer positions would deliver nonzero averages of the spin-correlations and add up to a final positive value when ${V_{ij}}^2$ is summed up. The inset of Figure 6 shows the mean fluctuation of the monomer coordinates about their average positions. These fluctuations do only mildly drop between $T = 5$ and $T = 1.5$ and much faster upon further reduction of the temperature. This is easily explained with the theta transition of the system, during which the brush is collapsing (Figure 5, inset). As a consequence of the collapse, the monomer fluctuations are reduced and the Vassiliev−Matsen order parameter is increasing rapidly. Therefore, this order parameter displays the theta transition rather than the ODT, which explains the much lower transition temperature obtained with this method.

## IV. Pattern Engineering through Shear

In Figure 1, the upper right snapshot displays stripelike "ripples" microdomains, but unlike similar results obtained with SCF methods,[29] the pattern is rather irregular as also known for thin films of block copolymers[30] and of adsorbed monolayers[31] and experimental results.[7,8] A possible strategy to increase long-range order is to apply a shear field using a lateral solvent flow over the layer. Note that such is possible for mixed polymer brushes but not for diblock copolymer thin films since the latter would be delaminated by the flow.

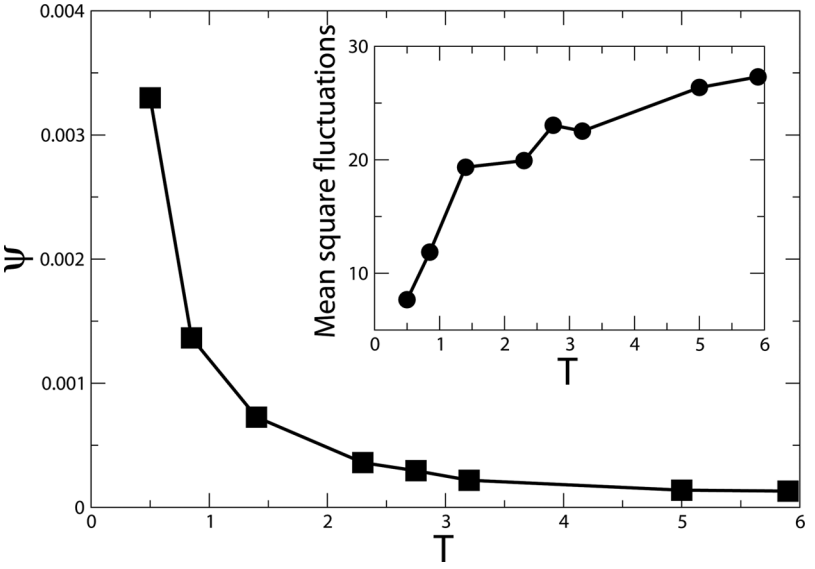


**Figure 6.** Order parameter as defined in eq 9, plotted against the temperature of the system (grafting density: $\sigma = 0.12$). Inset: average mean-square fluctuation of the monomers.

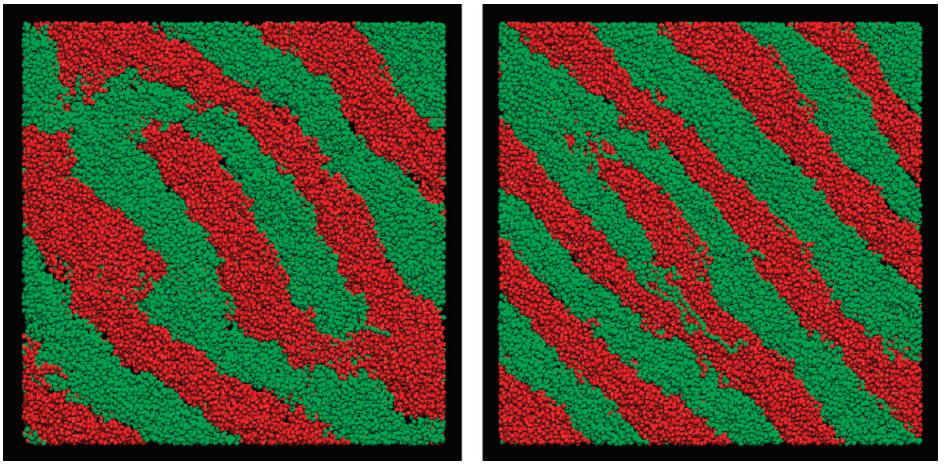

**Figure 7.** Binary brushes under shear flow in the diagonal direction. The force acting on the floating particles was $f = 0.14$ (left) and $f = 0.71$ (right). Apart from the flow, system parameters were identical to the brush in Figure 1 (upper-right panel).

While implementing the flow in the simulations, we did not try to simulate a correct hydrodynamics using a correspondingly dense (explicit) solvent. Instead, in order to reduce the computational effort and to focus on the main effect, namely the transfer of momentum from the flow field to the polymer layer, freely floating particles were added to the system and accelerated through a uniform external field. While colliding with the monomers, they transferred their momenta to the brush layer. In order to confine the "flow" particles, an upper wall was implemented at the vertical coordinate $z = 75\sigma_b$, far above the brush surface to avoid any spurious boundary effects. The particles were given the mass $m = 0.2$ and size $d = 0.25$ and accelerated by external forces of the magnitude $f = k\sqrt{2}$ in the diagonal direction, with $k \in \{0.1, 0.2, ..., 0.5\}$ (all units are LJ units). The particles were interacting with the monomers through a LJ potential, which was cut off at its minimum to leave only the repulsive part. The number of particles was equal to the number of monomers, but their volume fraction was a factor of 64 smaller due to their smaller size. In order to investigate whether the grafting pattern has got any influence on the pattern of the microphases, two different grafting patterns of brushes were simulated: first, the checkerboard pattern which was used for the brushes in the previous sections and, second, a randomly occupied Cartesian grafting pattern. The chain length was $N = 64$, and the grafting density was $\sigma = 0.12$.

Figure 7 displays snapshots of the system under different conditions. When compared to Figure 1 (upper-right panel), which shows the same system without flow, the impact of flow on the regularization of the domain pattern is clearly visible. A quantitative analysis of the domain structure is obtained with the structure factor, eq 4, which was evaluated in the same manner as described in section IIIB, with one exception: The structure factor is evaluated only in the diagonal direction perpendicular to the stripe pattern (or, equivalently, to the shear flow direction). The scattering vector is

$$\mathbf{q}_x = \mathbf{q}_y = \frac{2\pi n}{L}, \quad 0 \le n \le L \tag{11}$$

The results are shown in Figure 8 (upper panel). The plot shows that the average size of the stripes is gradually decreasing with increasing flow intensity $f$; i.e., a strong flow is inducing a larger number of stripes. The contrast of the stripe pattern, expressed

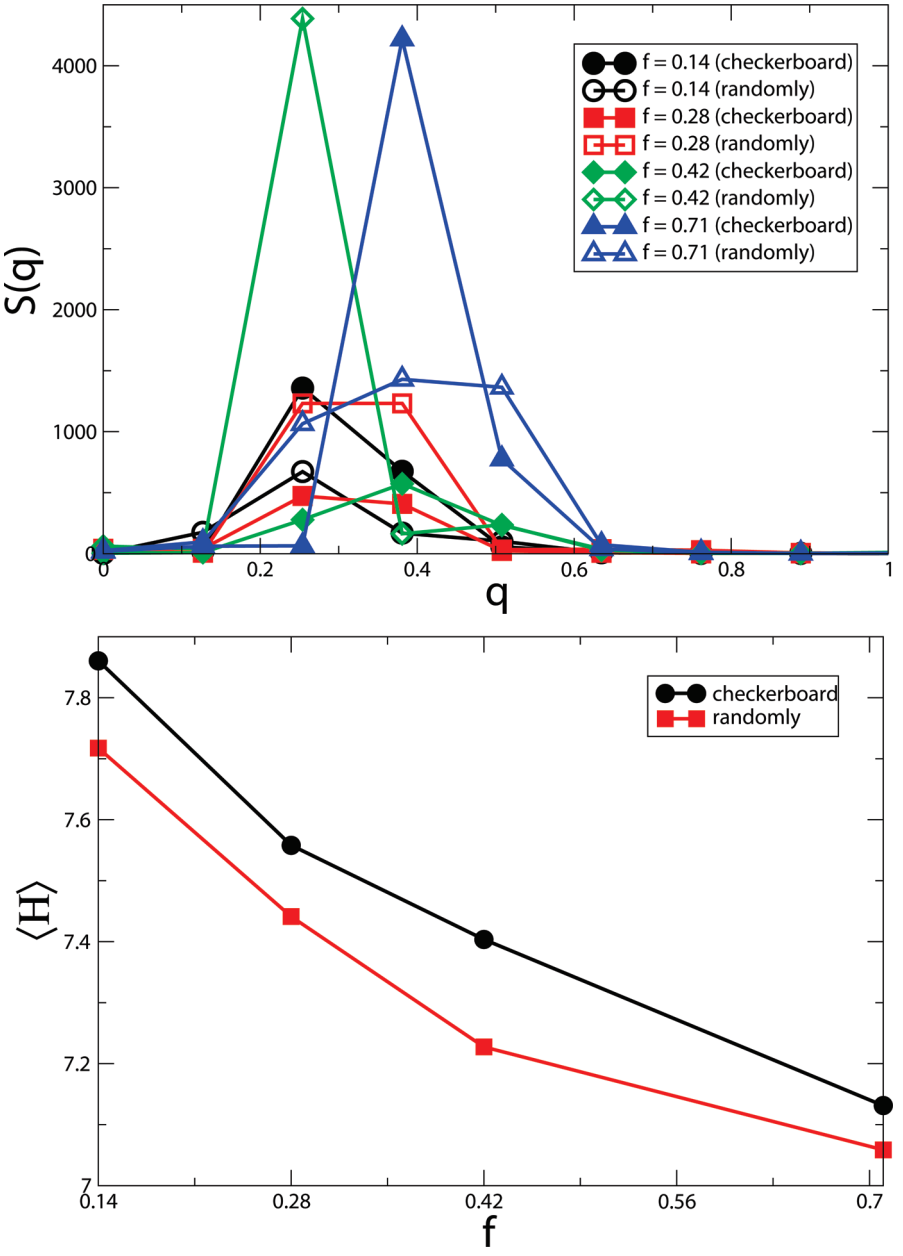


**Figure 8.** Upper panel: the structure factor, eq 4, at $\sigma = 0.12$ and $T = 0.5$ for different strengths of the shear flow. The forces $f$ refer to the floating particles (see text). Solid symbols: checkerboard grafting pattern; blank symbols: random grafting pattern. Lower panel: the average height (vertical center of mass) of the brush as a function of the shear flow strength for two different grafting patterns.

through the peak height of the structure factor, is also generally increasing with the flow. This is the case for both grafting patterns, although large fluctuations of the results are visible as well: At the highest flow intensity, $f = 0.71$, the checkerboard system (solid triangles) delivered a significantly stronger signal than the random system (blank triangles). At the moderate flow intensity, $f = 0.41$, the result was the opposite (solid and blank diamonds). Here it has to be acknowledged that the scattering factor is quite sensitive to random distortions of the stripe pattern and that the system size is fairly small so that a proper averaging over a sufficient number of stripes is difficult.

The lower part of the same figure displays the brush thickness (vertical position of the center of mass) $\langle H \rangle$ as a function of the shear force $f$ imposed on the particles. Generally, the height, in both grafting patterns, is decreasing with increasing force, which is understandable since the chains have to bend away from their grafting points when they experience the shear, and the finite stretching condition implies the reduction of their height. The randomly grafted brush height is systematically lower by a small amount of the order of 1%, which might be the result of a slightly different average chain interaction when compared with the checkerboard pattern. One may also notice that the brush height for $f = 0.14$ is a little bit larger than the height without shear. This is a spurious effect, generated by the presence of the floating particles, which are adsorbed into the brush body and, through their excluded volume contribution, increase the density of the system by a small amount and hence the average chain stretch.

## V. Conclusion

In this work, the ODT of a symmetric binary brush was investigated in detail. Several different approaches to analyze the transition behavior of this system have been compared. The structure factor (section IIIB), the pair-correlation function (section IIIC), and an analysis of the conformational deviations of the chains in section IIID consistently indicate a smooth

transition which takes place near a temperature of $T \approx 2.3$. An application of the Vassiliev−Matsen order parameter in section IIIE delivered a different result, which could be identified as the theta transition of the system, during which the brush is partially collapsing.

In the high temperature limit, the two species were homogeneously distributed in the brush; upon lowering the temperature, a microphase separation was taking place. Such a behavior had been predicted in the theoretical studies of the (laterally mobile) case of micelles with mixed corona.[10] The main difference of the micelle system to the polymer brushes investigated in the current paper is the lack of mobility of the grafting points on the substrate in the latter system. Hence, while the micelles were allowed to develop complete phase separations and, through intermicellar exchange, even modify their polymer compositions, our polymer brushes did only exhibit microdomains with a globally invariant (symmetric) composition.

Contrary to results of SCF calculations on similar systems,[14,29] the microphase separation generates an irregular stripe pattern rather than highly regular domains. This is in agreement with experimental observations[7] and a result of thermal fluctuations which were neglected in the SCF approach. At low temperature ($T = 0.5$), the "stripes" aligning in the diagonal direction were found more stable than what was discussed in ref 29, the separation either only in the $x$ direction or in both $x$ and $y$ directions forming a larger "checkerboard" pattern. Since the grafted approach has the same weight for two species in $x$ and $y$ directions, the "stripes" prefer to lying diagonally. Although the pattern in Figure 15 of ref 29 aligns in $x$ and $y$ equivalently ("checkerboard"), it will increase more phase boundary line tension than the diagonal "stripes" in our work. Furthermore, in section IV we demonstrate how an external flow imposed on the solvent could support a regularization of the domain pattern. Those regular stripes are of significant interest because they allow the generation of periodic surface potentials on nanoscales, and the switching of mixed brushes with hydrophilic and hydrophobic polymers upon change of solvent quality has recently been analyzed by the authors.[19]

**Acknowledgment.** This work was partly supported by the National Science Foundation of China under Grant 10225420. G.-L. He thanks J.-U. Sommer for the hospitality during a research stay at IPF Dresden.

## References and Notes

(1) Liu, Y.; Chen, X.; Xin, J. *Nanotechnology* **2006**, *17*, 3259.
(2) Li, N.; Veldhuis, S. C.; Yamamoto, K. *Mach. Sci. Technol.* **2007**, *11*, 45.
(3) Creton, C. *MRS Bull.* **2003**, *28*, 434.
(4) Sidorenko, A.; Minko, S.; Schenk-Meuser, K.; Duschner, H.; Stamm, M. *Langmuir* **1999**, *15* (24), 8349.
(5) S. Minko, D. U. E. G.; Stamm, M. *Macromol. Rapid Commun.* **2001**, *22*, 206.
(6) Lemieux, M.; Usov, D.; Minko, S.; Stamm, M.; Shulha, H.; Tsukruk, V. *Macromolecules* **2003**, *36*, 7244.
(7) Minko, S.; Mueller, M.; Usov, D.; Scholl, A.; Froeck, C.; Stamm, M. *Phys. Rev. Lett.* **2002**, *88*, 035502.
(8) Uhlmann, P.; Ionov, L.; Houbenov, N.; Nitschke, M.; Grundke, K.; Motornov, M.; Minko, S.; Stamm, M. *Prog. Org. Coat.* **2006**, *55*, 168.
(9) Halperin, A. *Europhys. Lett.* **1987**, *4* (4), 439.
(10) Halperin, A. *J. Phys.* (*Paris*) **1988**, *49*, 131.
(11) Marko, J.; Witten, T. *Phys. Rev. Lett.* **1991**, *66* (11), 1541.
(12) Marko, J.; Witten, T. *Macromolecules* **1992**, *25*, 296.
(13) Mueller, M. *Phys. Rev. E* **2002**, *65*, 030802.
(14) Zhulina, E.; Balazs, A. C. *Macromolecules* **1996**, *29*, 2667.
(15) Leibler, L. *Macromolecules* **1980**, *13*, 1602.
(16) Soga, K. G.; Zuckermann, M. J.; Guo, H. *Macromolecules* **1996**, *29*, 1998.
(17) Wenning, L.; Mueller, M.; Binder, K. *Europhys. Lett.* **2005**, *71*, 639.
(18) Santer, S.; Kopyshev, A.; Donges, J.; Ruehe, J.; Jiang, X.; Zhao, B.; Mueller, M. *Langmuir* **2007**, *23*, 279.
(19) Merlitz, H.; He, G.-L.; Sommer, J.-U.; Wu, C.-X. *Macromolecules* **2009**, *42*, 445.
(20) Chervanyov, A.; Heinrich, G. *J. Chem. Phys.* **2006**, *125*, 084703.
(21) Kremer, K.; Grest, G. *J. Chem. Phys.* **1990**, *92*, 5057.
(22) Plimpton, S. *J. Comput. Phys.* **1995**, *117*, 1 (http://lammps.sandia.gov/).
(23) He, G.; Merlitz, H.; Sommer, J.; Wu, C. *Eur. Phys. J. E* **2007**, *24*, 325.
(24) Hoffmann, A.; Sommer, J.-U.; Blumen, A. *J. Chem. Phys.* **1997**, *106*, 6709.
(25) Strobl, G. *The Physics of Polymers* , 3rd ed.; Springer: Berlin, 2007.
(26) Brazovskii, S. *Sov. Phys. JETP* **1975**, *41* (85).
(27) Merlitz, H.; He, G.-L.; Wu, C.-X.; Sommer, J.-U. *Macromolecules* **2008**, *41*, 5070.
(28) Vassiliev, O.; Matsen, M. *J. Chem. Phys.* **2003**, *118* (16), 7700.
(29) Dong, H. *J. Phys. II* **1993**, *3*, 999.
(30) Mansky, P.; Russell, T. P.; Hawker, C. J.; Mays, J.; Cook, D. C.; Satija, S. K. *Phys. Rev. Lett.* **1997**, *79* (2), 237.
(31) Pugnaloni, L.; Ettelaie, R.; Dickinson, E. *J. Colloid Interface Sci.* **2005**, *287*, 401.